Communications in Mathematics and Applications
Vol. 14, No. 2, pp. 981–999, 2023
ISSN 0975-8607 (online); 0976-5905 (print)
Published by RGN Publications
DOI: 10.26713/cma.v14i2.2111

http://www.rgnpublications.com

Research Article

Study of Activation Energy of Magnetohydrodynamic Radiative Casson Nanofluid With Darcy-Forchheimer Flow and Cattaneo-Christov Heat Flux Model

Mohammed Younus*[1], A. Venkatalakshmi[2] and Vajja Ramesh[3]

[1] *Department of Mathematics, Keshav Memorial Institute of Technology, Hyderabad, Telangana, India*
[2] *Department of Mathematics, University College of Science, Osmania University, Hyderabad, Telangana, India*
[3] *Department of Mathematics, Osmania University, Hyderabad, Telangana, India*
***Corresponding author:** younus@kmit.in

Received: November 4, 2022 **Accepted:** March 3, 2023

Abstract. In the present paper, the *Activation Energy* (AE) of a radiative *magnetohydrodynamic* (MHD) Casson nano fluid with Darcy-Forchheimer flow, and Cattaneo-Christov heat flux model across a linearly stretched sheet under convective boundary conditions was numerically explored. The influence of different factors on profiles of temperature, velocity, and concentration was investigated and graphically interpreted. The acquired results are extremely similar to those found in the open literature. The profile of velocity was observed for porosity parameter, Casson fluid parameter, Forchheimer parameter, and magnetic parameter. The temperature profile was observed for porosity parameter, Forchheimer parameter, Brownian motion parameter, magnetic parameter, thermophoresis parameter, Casson fluid parameter, Biot number, thermal relaxation parameter, and radiation parameter. The concentration profile was examined for porosity parameter, *Activation Energy* (AE), temperature difference, thermophoresis parameter, chemical reaction rate constant, parameter of Brownian motion, and Lewis number. Also, local Nusselt number, coefficient of skin friction, and local Sherwood number were found for different parameters.

Keywords. Activation energy, Casson nano fluid, Darcy-Forchheimer flow, Shooting method, Cattaneo-Christov heat flux

Mathematics Subject Classification (2020). 76M55, 76M20, 76A05, 76S05, 65L06, 65L10, 80A21, 80A32

1. Introduction

The large range of applications drew engineers, researchers, and scientists to examine "mass and heat transfer of boundary layer flow of non-Newtonian fluids over stretching surfaces". Svante Arrhenius invented in 1889 the term "Arrhenius activation". It mimics the lowest energy required to produce a chemical reaction in a chemical system including potential reactants (Huang [18]). The *Activation Energy* (AE) is the least quantity of energy, chemical reactants require to produce a chemical reaction (Abbas and Magdy [1]). The impact of AE on "convective heat and mass transmission in the boundary layer region" was explored by Bestman [6]. Several experiments have been done since then to see how AE impacts mass and heat transmission in the boundary layer flow of fluid. Anuradha and Sashikala [2], and Dhlamini *et al*. [12] investigated the effect of AE on mass and heat transmission in fluid flow that is not stable under varied geometries. In the boundary layer flow of MHD, Huang [18], and Mustafa *et al*. [26] investigated the influence of AE on nano fluids passing through a porous horizontal cylinder. Majeed *et al*. [22] investigated the activation energy in the MHD flow using momentum slip model of a second-order and a chemical process. The flow of Casson hybrid nanofluid over a plate moving vertically with the impact of magnetic and Arrhenius activation energy in convective boundary conditions was investigated by Sarwe *et al*. [37]. Magnetohydrodynamic Casson nanofluid along with activation energy under the effect of thermal conductivity that is temperature dependent, exponential and variable viscosity over a stretching surface was investigated by Atif *et al*. [4]. Sarve *et al*. [36] looked at the effect of activation energy on Casson fluid Darcy-Forchheimer flow with nano particles. Sajid *et al*. [35] examined Maxwell nanofluid Darcy-Forchheimer flow on a linearly stretching surface. They considered nonlinear thermal radiation, activation energy (AE), and variable thermal conductivity in the heat and mass transport study. Through entropy generation, Shah *et al*. [38] investigated *Activation Energy* (AE), and chemical reaction over nonlinearly expanding surfaces in MHD Casson nanofluid flow with radiation affects. Devi *et al*. [11], Dhlamini *et al*. [12], and Jawad *et al*. [21] discuss additional research on the impact of AE on non-Newtonian fluids under various surfaces. According to their statistics, the nanoparticle concentration increases as the value of activation energy (AE) rises.

Porous media is a type of porous material with pores that are normally filled with fluid. Engineers, mathematicians, geologists, and architects are all fascinated by the notion of fluid flow in porous media because of its many applications, including water flow in reservoirs, heat exchangers, Catalytic reactors, and oil production. Heat transmission in porous media is widely employed in the manufacture of papers, electrical technology, nonwoven things, heat pipe technology as well as energy storage, among other things (Sajid *et al*. [35]). During the study in 1856 regarding the flow of water through sand beds, groundwork for the flow of homogenous fluids across porous media was laid by a French civil engineer, H. Darcy. When both boundary effect and inertial effect occur at higher flow rate, law of Darcy does not perform properly. Later, in 1901, a Dutch scientist, Philippe's Forchheimer, modified the velocity expression of Darcian by including the squared velocity term in the equation of momentum to forecast inertia and boundary layer flow. Ganesh *et al*. [14] inspected the temperature profile of MHD nano fluid with Darcy-Forchheimer flow over shrinking / stretching sheet when the effect of viscous dissipation is present. Muhammad *et al*. [24] recent work on the Darcy-Forchheimer (Sajid

et al. [35]) Maxwell nanofluid flow under zero mass flux, and convective boundary conditions across an elongating sheet utilizing porous media revealed that enhancing the value of the porosity parameter inclines the temperature and nanoparticle concentration profile. With the use of the *homotopy analysis method* (HAM), Aziz *et al*. [5] numerically addressed the flow of third grade fluid which is unsteady over a flat porous plate entrenched in a porous medium. They found a decrease in the field of concentration as the Schmidt number grew. Ramesh [31] observed 3D Casson nano liquid flow in two lateral directions over a porous region via Darcy-Forchheimer articulation that takes into account the impact of uniform heat sink/source as well as boundary condition which is convective. Hayat *et al*. [16] studied about Darcy-Forchheimer flow with mixed convection that is nonlinear. Bilal *et al*. [7] studied the hybrid nanofluid's Darcy-Forchheimer mixed convection flow through an inclined expanding cylinder.

Fourier (1822) took the initiative to study the mechanism of heat transport in various practical areas with his heat flow model, often known as the heat conduction law. This law causes the formation of the parabolic heat equation, which illustrates how the considered system is immediately impacted by the first generated disturbance. The result is in direct conflict with the idea of heat conduction. Numerous changes have been made to law of heat conduction by Fourier (cf. Jabeen *et al*. [20]) to address this issue. One of these was the heat conduction law proposed by Cattaneo (1948) by including thermal relaxation time. This change produced a hyperbolic equation that allows for the transmission of waves for the transportation of energy. Activation energy with Cattaneo-Christov heat flux under various boundary settings were explored by Eswaramoorthi *et al*. [13], Ijaz *et al*. [19], and Muhammad *et al*. [24]. Prasad *et al*. [28], Reddy *et al*. [34], and Ramana *et al*. [30] studied about Cattaneo-Christov heat flux theory on different fluids under various conditions. Darcy-Forchheimer nano fluid flow with the theory of heat and mass flux given by Cattaneo-Christov on non-linearly stretching surface was investigated by Rasool and Zhang [32].

The flow of nano liquid over an elongated sheet in several physical phases was then investigated by a number of researchers (Gangaiah *et al*. [15], and Maleque [23]). In 1959, Casson [8] presented a viscoelastic fluid model that became the model which is called as the Casson fluid model. Casson fluid is a liquid that thins as it is sheared. At an infinite shear rate, there is no viscosity and a viscosity of infinity at zero shear rate, yield stress less than which no flow occurs (Dash *et al*. [10]). Investigations of Charm and Kurland [9], and Walwander *et al*. [41] on blood with various hematocrits, anticoagulants, and temperatures clearly showed that blood behaves like a Casson fluid. Some recent research of Arthur *et al*. [3], Gangaiah *et al*. [15], Jawad *et al*. [21], Rafique *et al*. [29], and Thamaraikannan *et al*. [39] are particularly interested in the nature of Casson fluid under different boundary conditions and different stretching surfaces.

In present work, we explored the impact of *Activation Energy* (AE) of MHD Casson nanofluid with Darcy-Forchheimer flow and Cattaneo-Christov heat flux model under convective boundary conditions over a linear stretching sheet. The results of the Nusselt number, Sherwood number, and coefficient of skin friction were presented numerically in tables and discussed graphically in detail regarding dimensionless temperature, velocity, and concentration.

2. Mathematical Formulation

Here we consider 2D boundary layer incompressible, steady, laminar flow of MHD Casson fluid with Darcy-Forchheimer porous medium over a linear stretching sheet with the effect of radiation. Coordinate 'x' is taken along the sheet with u as the velocity component and 'y' is taken normal to the sheet with v as the velocity component. The stretching sheet causes the flow to occur. Keeping the origin fixed, the sheet is then stretched with a linear velocity $U_W(x) = ax$, where 'a' is a positive constant associated with the stretching sheet. While maintaining the origin stationary, convective heat is applied to the sheet's surface. In the y-direction, a consistent magnetic field B_0 is applied. Cattaneo-Christov model is used to study the significances of activation energy.

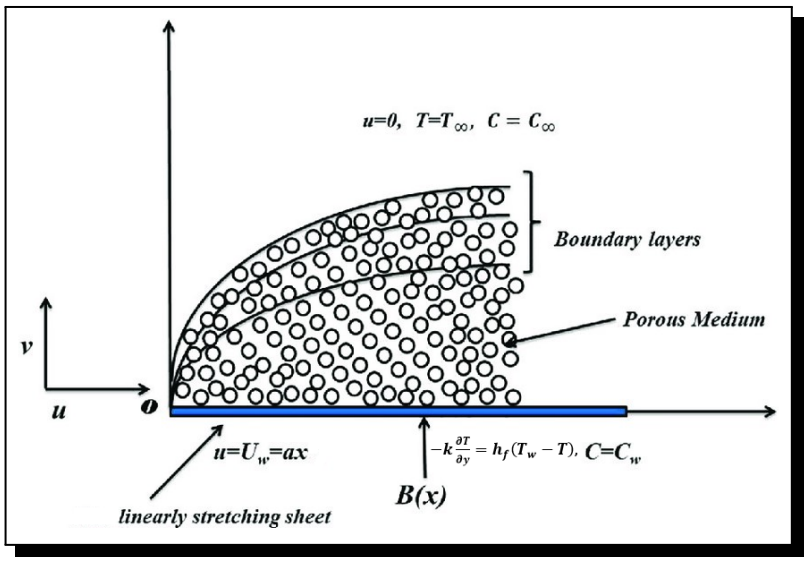

Figure 1. Fluid flow physical model

The equations for momentum, temperature, and concentration under the aforementioned conditions are written as (Atif *et al*. [4], Eswaramoorthi *et al*. [13], Gangaiah *et al*. [15], and Sajid *et al*. [35]):

The equation of continuity is

$$\frac{\partial u}{\partial x} + \frac{\partial v}{\partial y} = 0. \tag{1}$$

The equation of momentum is

$$u\frac{\partial u}{\partial x} + v\frac{\partial u}{\partial y} = \nu\left(1 + \frac{1}{\beta}\right)\frac{\partial^2 u}{\partial y^2} - \frac{\nu}{k_1}u - \frac{c_b}{x\sqrt{k_1}}u^2 - \frac{\sigma {B_0}^2}{\rho_f}u. \tag{2}$$

The equation of energy is

$$u\frac{\partial T}{\partial x} + v\frac{\partial T}{\partial y} + \lambda_T\omega_T = \frac{k}{\rho_f c_p}\frac{\partial^2 T}{\partial y^2} - \frac{1}{\rho c_p}\frac{\partial q_r}{\partial y} + \tau\left[D_B\frac{\partial C}{\partial y}\frac{\partial T}{\partial y} + \frac{D_T}{T_\infty}\left(\frac{\partial T}{\partial y}\right)^2\right]. \tag{3}$$

The equation of concentration is

$$u\frac{\partial C}{\partial x} + v\frac{\partial C}{\partial y} + \lambda_C\omega_C = \frac{D_T}{T_\infty}\frac{\partial^2 T}{\partial y^2} + D_B\frac{\partial^2 C}{\partial y^2} - {k_r}^2(C - C_\infty)\left(\frac{T}{T_\infty}\right)^n e^{-\left(\frac{E_a}{kT}\right)}, \tag{4}$$

where

$$\omega_T = u\frac{\partial u}{\partial x}\frac{\partial T}{\partial x} + v\frac{\partial v}{\partial y}\frac{\partial T}{\partial y} + u^2\frac{\partial^2 T}{\partial x^2} + v^2\frac{\partial^2 T}{\partial y^2} + 2uv\frac{\partial^2 T}{\partial x \partial y} + u\frac{\partial v}{\partial x}\frac{\partial T}{\partial y} + v\frac{\partial u}{\partial y}\frac{\partial T}{\partial x} \tag{5}$$

and

$$\omega_C = u\frac{\partial u}{\partial x}\frac{\partial C}{\partial x} + v\frac{\partial v}{\partial y}\frac{\partial C}{\partial y} + u^2\frac{\partial^2 C}{\partial x^2} + v^2\frac{\partial^2 C}{\partial y^2} + 2uv\frac{\partial^2 C}{\partial x \partial y} + u\frac{\partial v}{\partial x}\frac{\partial C}{\partial y} + v\frac{\partial u}{\partial y}\frac{\partial C}{\partial x}. \tag{6}$$

The boundary conditions are (Younus and Lakshmi [43]):

$$\left.\begin{array}{l} \text{At } y = 0,\ u = U_w = ax,\ v = 0,\ -k\frac{\partial T}{\partial y} = h_f(T_w - T), \text{ and } C = C_w, \\ \text{As } y \to \infty,\ u \to 0,\ T \to T_\infty, \text{ and } C \to C_\infty. \end{array}\right\} \tag{7}$$

Fluid density is denoted with ρ_f, viscosity coefficient with μ, $\beta = \mu_B \frac{\sqrt{2\pi_c}}{P_y}$ represents the Casson fluid parameter (Gangaiah *et al*. [15]), C and T represents fluid's concentration and fluid's temperature, T_∞, C_∞ represents the ambient temperature of fluid and concentration respectively, σ is the fluid electrical conductivity, k denotes the thermal conductivity and at constant pressure, "the specific heat of the fluid" is denoted with c_p, $\nu = \frac{\mu}{\rho_f}$ is the kinematic viscosity, $\tau = \frac{(\rho c)_p}{(\rho c)_f}$ represents ratio of nanoparticle's heat capacity to heat capacity of base fluid, D_B and D_T are the 'Brownian motion, and thermal diffusion coefficients', k_1 denotes permeability of porous medium, c_b stands for drag coefficient, λ_T, $\lambda_C$represents relaxation time of heat and mass flux, respectively (Eswaramoorthi *et al*. [13]). In the boundary conditions, convective heat transfer coefficient denoted by h_f, "convective fluid temperature" at the sheet represented by T_w, k_r is considered as a "parameter of response rate" 'n' is the fitted rate constant and E_a is the activation energy.

The radiative heat flux q_r with Roseland's approximation for radiation, can be written as

$$q_r = \frac{-4 \propto^1}{3k^1}\frac{\partial T^4}{\partial y}. \tag{8}$$

Here $\propto^1$ is Stefan-Boltzmann constant, k^1 denoting coefficient of absorption. Assuming that the temperature T changes in the flow, T^4 may be taken as a 'linear function' of T. By ignoring terms having order greater than one in Taylor's series expansion for T^4 about T_∞, (Atif *et al*. [4]) we get

$$T^4 \cong {T_\infty}^3(4T - 3T_\infty). \tag{9}$$

By substituting (9) in (8), we get

$$q_r = \frac{-16 \propto^1}{3k^1}T_\infty^3\frac{\partial T}{\partial y}. \tag{10}$$

2.1 Method of Solution

Using the similarity transformations shown below, we can get a system of ODE from a system of PDE.

$$\left.\begin{array}{l} \eta(x,y) = \sqrt{\frac{a}{\nu}}y,\ \psi(x,y) = \sqrt{a\nu}f(\eta), \\ T = T_\infty + (T_w - T_\infty)\theta(\eta),\ C = C_\infty + (C_w - C_\infty)\phi(\eta), \end{array}\right\} \tag{11}$$

where η denotes "the similarity variable", $\psi(x,y)$ denotes "the stream function", $f(\eta)$, $\phi(\eta)$, and $\theta(\eta)$ denotes stream function, concentration function, and temperature function respectively.

The continuity equation is getting satisfied by picking $\psi(x,y)$ such that $u=\frac{\partial\psi}{\partial y}$, $v=-\frac{\partial\psi}{\partial x}$, and therefore

$$u=axf'(\eta),\quad v=-\sqrt{a\nu}f(\eta). \tag{12}$$

The equations (1)-(4) can be transformed into a system of ODE with the above conversions (12).

$$\left(1+\frac{1}{\beta}\right)f'''(\eta)+f(\eta)f''(\eta)-F_r[f'(\eta)]^{2\cdot}-[f'(\eta)]^{2\cdot}-\lambda f'(\eta)-Mf'(\eta)=0, \tag{13}$$

$$\theta''(\eta)+\frac{4R}{3}\theta''(\eta)-Pr\delta_T[f(\eta)]^2\theta''(\eta)+Prf(\eta)\theta'(\eta)+PrN_b\theta'(\eta)\phi'(\eta)+PrNt\left[\theta'(\eta)\right]^2 -Pr.\delta_T.f(\eta).f'(\eta).\theta'(\eta)=0, \tag{14}$$

$$\phi''(\eta)-\phi''(\eta)LePr\delta_C[[f(\eta)]^2+LePrf(\eta)\phi'(\eta)+\frac{Nt}{Nb}\theta''(\eta)-LePr\delta_Cf(\eta).f'(\eta).\phi'(\eta) -\sigma^*LePr\ e^{-\left(\frac{E}{1+\theta\delta}\right)}(1+\theta\delta)^n\phi(\eta)=0. \tag{15}$$

As a result, the dimensionless boundary conditions (7) are created.

$$\left.\begin{aligned} &f(\eta)=0,\ f'(\eta)=1,\ \theta'(\eta)=Bi[\theta(\eta)-1],\text{ and }\ \phi(\eta)=1\text{ at }\eta=0,\\ &\text{and }\ f'(\eta)\to 0,\ \theta(\eta)\to 0,\text{ and }\phi(\eta)\to 0\text{ as }\eta\to\infty, \end{aligned}\right\} \tag{16}$$

$F_r=\frac{c_b}{\sqrt{k_1}}$ is the Forchheimer parameter (Sajid *et al*. [35]), $\lambda=\frac{\nu}{k_1a}$ is the porosity parameter, $Pr=\frac{\mu}{k}c_p=\frac{\nu}{\alpha}$ is the Prandtl number, $M=\frac{\sigma{B_0}^2}{a\rho_f}$ represents the magnetic field parameter, $Nb=\frac{\tau D_{B(C_w-C_\infty)}}{\nu}$ denotes the Brownian motion parameter, $\delta_T=a\lambda_T$ is Thermal Relaxation parameter, $Le=\frac{\alpha}{D_B}$ is the Lewis number, $Nt=\frac{\tau D_{T(T_w-T_\infty)}}{\nu T_\infty}$ represents the thermophoresis factor, $Bi=\frac{h_f}{k}\sqrt{\frac{\nu}{a}}$ is the Biot number, $\delta_C=a\lambda_C$ is Solute Relaxation parameter $\sigma^*=\frac{{k_r}^2}{a}$ is denoting the reaction rate constant, $E=\frac{E_a}{kT_\infty}$ is the AE and $\delta=\frac{(T_w-T_\infty)}{T_\infty}$ is the temperature difference. Cf_x denotes the coefficient of local skin friction, and local Nusselt number with Nu_x, and Sh_x for the local Sherwood number are defined as follows

$$Cf_x=\frac{\tau_w}{\rho{U_w}^2},\quad Nu_x=\frac{xq_w}{k(T_w-T_\infty)},\quad Sh_x=\frac{xq_m}{D_B(C_w-C_\infty)}. \tag{17}$$

Here $\tau_w=\mu[\frac{\partial u}{\partial y}]$ at $y=0$ denotes "the shear stress at the wall", $q_w=-k[\frac{\partial T}{\partial y}]_{y=0}$ and $q_m=-D_B[\frac{\partial C}{\partial y}]_{y=0}$ are "the heat transfer rate, and the mass transfer rate at the surface of the sheet". Using similarity transformations (11), the coefficient of local Skin friction, the local Nusselt number, and the local Sherwood number were transformed to (Eswaramoorthi *et al*. [13], and Gangaiah *et al*. [15])

$$(Re_x)^{\frac{1}{2}}Cf_x=\left(1+\frac{1}{\beta}\right)f''(0), \tag{18}$$

$$(Re_x)^{\frac{-1}{2}}Nu_x=-\left(1+\frac{4R}{3}\right)\theta'(0), \tag{19}$$

$$(Re_x)^{\frac{-1}{2}}Sh_x=-\phi'(0), \tag{20}$$

where $Re_x=\frac{xU_w}{\nu}$ is local Reynold's number.

2.2 Numerical Scheme

The set of equations (13)-(15) along with boundary settings (16) were solved numerically by Runge-Kutta (RK) Method with the help of shooting technique. The equations are first reduced into a system of differential equations of first order. Let's first take into consideration the following variables for this

$$\left.\begin{aligned} &f = f_1,\ f' = f_2,\ f'' = f_3, \\ &\theta = f_4,\ \theta' = f_5,\ \phi = f_6,\ \phi' = f_7 \end{aligned}\right\} \tag{21}$$

The system of *differential equations* (DEs) of order one is obtained by altering equations (13)-(15) using the variables indicated in (21).

$$f_1^1 = f' = f_2, \tag{22}$$

$$f_2^1 = f'' = f_3, \tag{23}$$

$$f_3^1 = f''' = \frac{[(1+F_r)(f_2)^2 - f_1 f_3 + (M+\lambda)f_2]]}{\left[1+\frac{1}{\beta}\right]}, \tag{24}$$

$$f_4^1 = \theta' = f_5, \tag{25}$$

$$f_5^1 = \theta'' = -\frac{Pr}{(1+\frac{4R}{3} - Pr\,\delta_T (f_1)^2)}[f_1 f_5 - \delta_T f_1 f_2 f_5 + Nb\, f_5 f_7 + Nt(f_5)^2], \tag{26}$$

$$f_6^1 = \phi' = f_7, \tag{27}$$

$$\begin{aligned} f_7^1 = \phi'' = \frac{1}{(1 - LePr\delta_C (f_1)^2)}\Bigg[&\frac{Nt}{Nb}\frac{Pr}{(1+\frac{4R}{3} - Pr\,\delta_T (f_1)^2)} \\ &\cdot [f_1 f_5 + Nb\, f_5 f_7 + Nt(f_5)^2 - \delta_T f_1 f_2 f_5] + LePr\sigma^* (1+\delta\theta)^n . e^{-\left(\frac{E}{1+\delta\theta}\right)}\phi(\eta) \\ &- Le\,.Pr\,.f_1 f_7 + LePr\delta_C f_1 f_2 f_7\Bigg]. \end{aligned} \tag{28}$$

The *boundary conditions* (BCs) are changed as follows

$$\left.\begin{aligned} &f_1(\eta) = 0,\ f_2(\eta) = 1,\ f_5(\eta) = Bi[f_4(\eta) - 1],\ f_6(\eta) = 1 \ \text{ for } \ \eta = 0 \\ &\text{and } \ f_2(\eta) \to 0,\ f_4(\eta) \to 0,\ f_6(\eta) \to 0 \ \text{ as } \eta \to \infty. \end{aligned}\right\} \tag{29}$$

To calculate $\theta'(0) = f_5(0)$, a value of $\theta(0) = f_4(0)$ is required to solve the above system of equations (22)-(28) with the above boundary conditions (29). However, such value was not set at the boundary. As a result, the proper guess functions for $f(\eta)$, $\theta(\eta)$ and $\phi(\eta)$ are chosen in order to get the values of $\theta(0)$ in the algorithm of MATLAB for the R-K method shooting approach with size of the step as $\Delta\eta = 0.01$. We have chosen the values $\eta_{\max} = 5$, $\theta(0) = 2$ to ensure that $\theta'(0) = 1$ and matched the values of $-\theta'(0)$ with the results prevailing. This particular process is continued till the results are converging within 10^{-4} tolerance limit (Younus *et al*. [43]).

3. Results and Discussion

Using the MATLAB program with RK method, we analysed the behaviour of temperature, velocity, nano particle volume fraction profile with relevant parameters. The findings are shown in Tables 1–5, and Figures 2–21. Throughout the analysis for graph plotting, and numerical data we used $\lambda = \delta = Fr = 0.3$, $\delta_C = \delta_T = 0.1$, $Le = 1.2$, $M = Nt = n = Nb = Bi = \sigma^* = 0.5$, $Pr = 6.9$, $R = 0.6$, $\beta = 0.8$, $E = 1$ except in few cases.

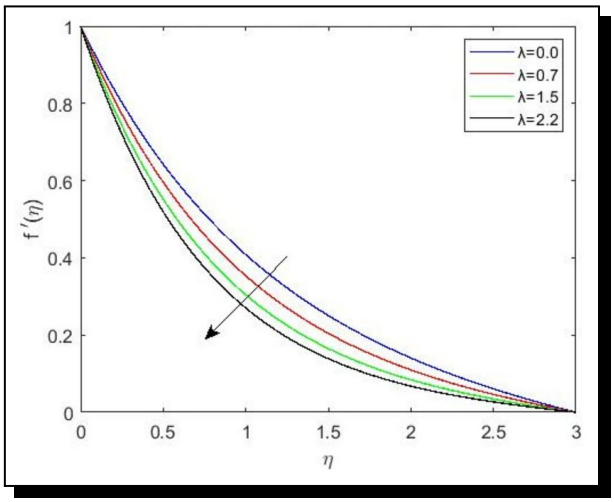

Figure 2. Variation in velocity for different λ values

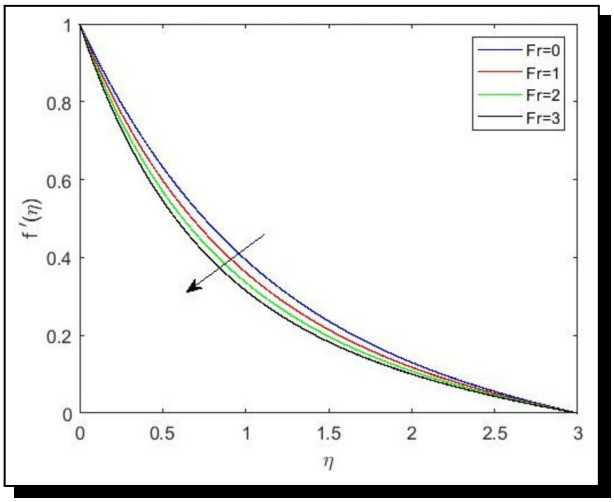

Figure 3. Variation in velocity for different Fr values

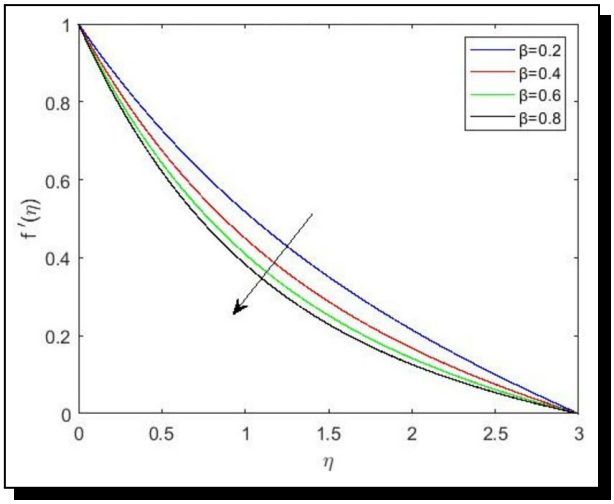

Figure 4. Variation in velocity for different β values

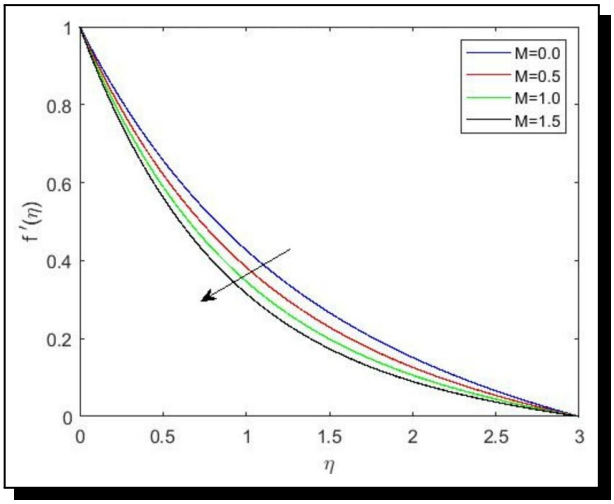

Figure 5. Variation in velocity for different M values

To emphasise the conclusions, we discussed in a physical sense the problem's graphical outputs. Effects of various parameters on the dimensionless velocity profiles are shown in Figures 2-5. Figure 2 demonstrates how the velocity profile changes as the porosity parameter ($0 \le \lambda \le 2.2$) is changed. The velocity profile appears to be declining as the value of porosity parameter is increased (Rasool and Zhang [32]). The higher the porosity parameter, the greater the resistance provided by the medium to fluid flow, resulting in a decrease in velocity. Figure 3 indicates that enhancing the value of the Forchheimer parameter ($0 \le Fr \le 3$) decreases the velocity profile. The thermal boundary layer grows thicker and fluid cannot move effortlessly as the Forchheimer parameter value is increased. The explanation for this behaviour is because the porous medium's inertia adds to fluid flow mechanism's resistance, causing the fluid to travel at a slower pace as the temperature rises. From Figure 4 it is clear that, enhancing the Casson fluid parameter value ($0.2 \le \beta \le 0.8$) lowers the velocity profile. Physically, an increased Casson value indicates a lower yield stress, which corresponds to a Newtonian fluid due to which

the fluid velocity is restricted. Increases in β cause the fluid viscosity to increase, reducing the velocity of the fluid. Figure 5 demonstrates how the velocity profile changes in relation to M ($0 \le M \le 1.5$) i.e. the magnetic parameter. Because of the magnetic field, the velocity profile drops when the magnetic parameter M is increased. The Lorentz force is generated by an electrically conducting fluid when a magnetic field is present. In the presence of Lorentz force, molecular collisions increase. The temperature of the fluid grows as a result, and the fluid's velocity inside the boundary layer decreases.

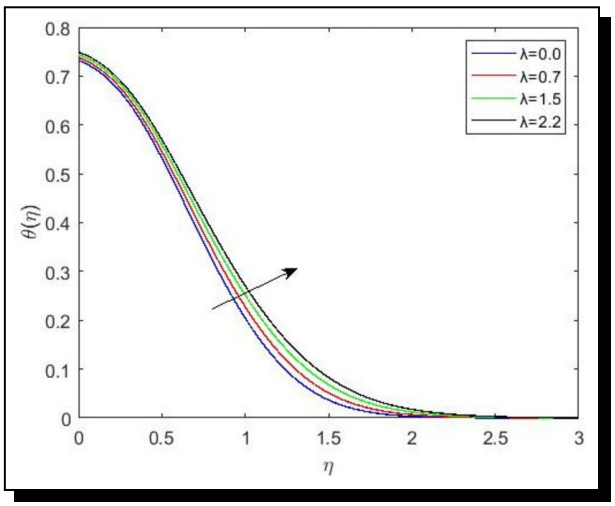

Figure 6. Variation in temperature for different λ values

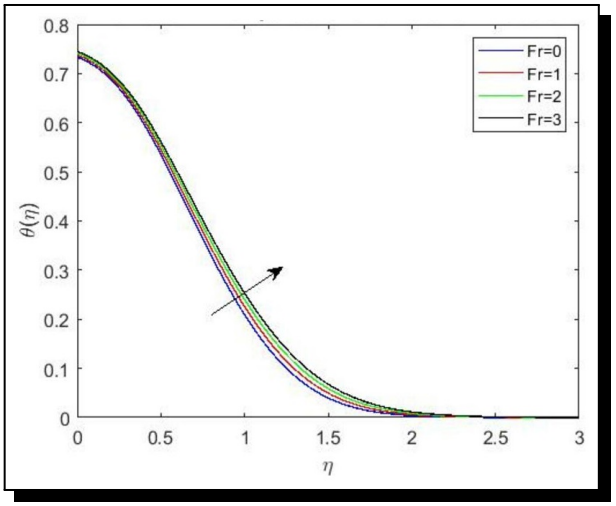

Figure 7. Variation in temperature for different Fr values

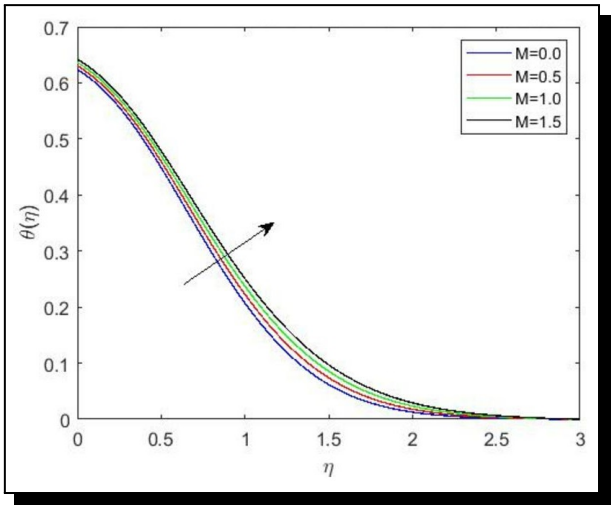

Figure 8. Variation in temperature for different M values

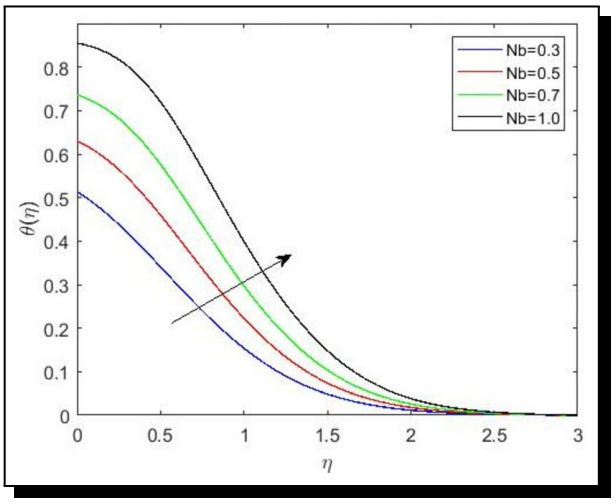

Figure 9. Variation in temperature for different Nb values

The effects of several parameters on profiles of temperature are shown in Figures 6-14. Figure 6 evaluates the link between the temperature profile and the porosity parameter ($0 \le \lambda \le 2.2$). As the parameter of porosity is increased, the temperature profile, and thermal layer thickness improve (Sajid *et al*. [35]). It has been discovered that porous media's presence causes an increase in the opposition to fluid flow, resulting in a stronger temperature profile.

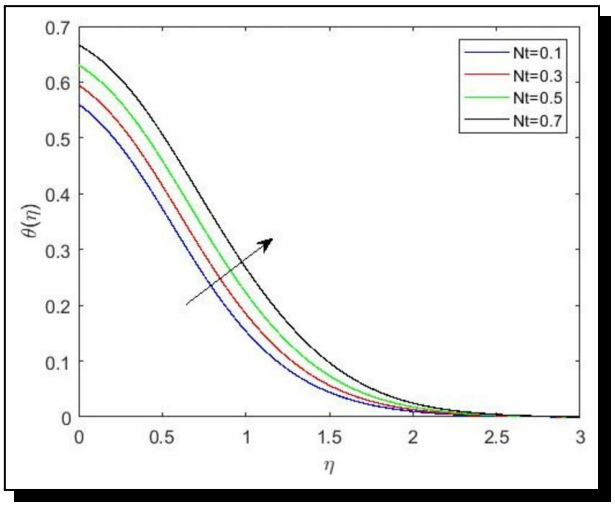

Figure 10. Variation in temperature for different Nt values

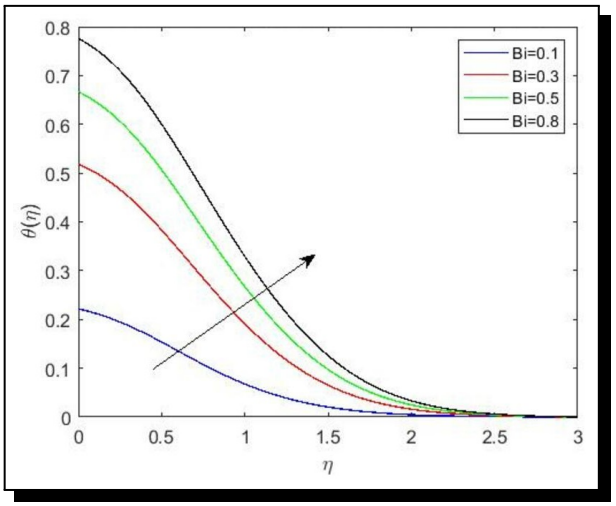

Figure 11. Variation in temperature for different Bi values

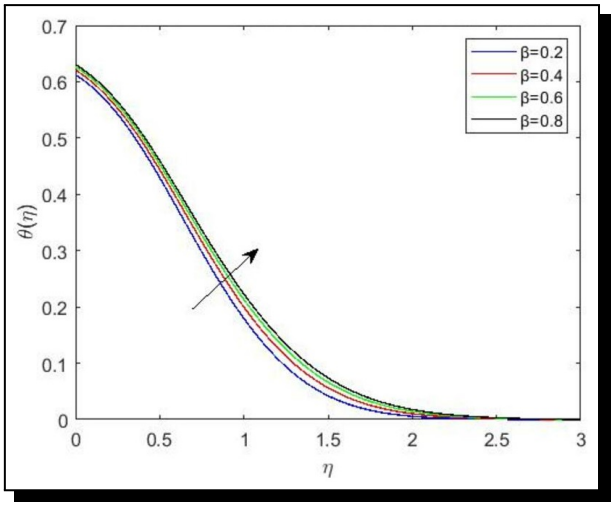

Figure 12. Variation in temperature for different β values

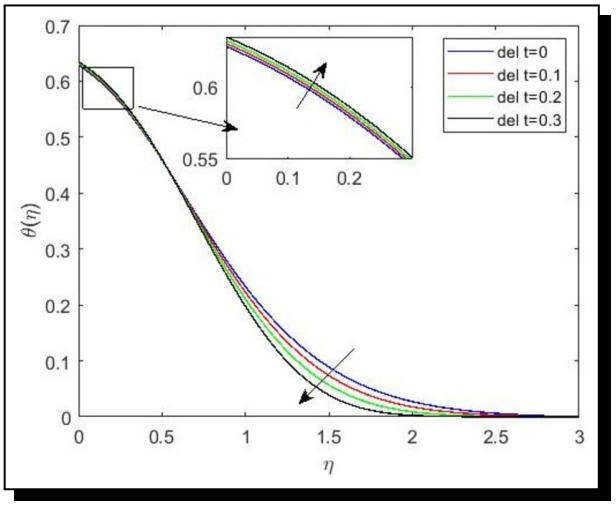

Figure 13. Variation in temperature for different δ_T values

In Figure 7, we can see that when the $(0 \leq Fr \leq 3)$ value rises, temperature rises, because the porous medium's inertia adds resistance to fluid flow mechanism. In Figure 8, the temperature profile is strengthened with an increase in magnetic parameter $(0 \leq M \leq 1.5)$ as the Lorentz force is present. The case in which $M \neq 0$ denotes hydromagnetic flow and $M = 0$ (Reddy *et al*. [34]) denotes hydrodynamic inertia adds resistance to fluid flow mechanism. In Figure 8, the temperature profile is strengthened with an increase in magnetic parameter $(0 \leq M \leq 1.5)$ as the Lorentz force is present. The case in which $M \neq 0$ denotes hydromagnetic flow and $M = 0$ (Sajid *et al*. [35]) denotes hydrodynamic flow. For the hydromagnetic scenario, the temperature profile is clearly higher than the temperature profile for the hydrodynamic case. From Figure 9, it's clear that the fluid temperature rises when the Brownian motion parameter $(0.3 \leq Nb \leq 1)$ is increased. As Nb levels grow, the zig-zag velocity of nanoparticles suspended in fluid increases, increasing the likelihood of collisions with molecules moving quickly and raising the temperature. The thermophoresis parameter's (Sajid *et al*. [35]) behaviour is depicted in Figure 10, where an

increase in the thermophoresis parameter Nt lying between 0.1 and 0.7 appears to raise the fluid temperature. The increase in nanoparticles is the cause of the temperature increase. When thermophoretic force is present, the thermal boundary layer thickens as nanoparticles at the hot boundary move towards the cool fluid (Mustafa *et al*. [26]). In Figure 11, the impact of "Biot number" ($0.1 \le Bi \le 0.8$) can be seen on temperature profile. The ratio between the heat transfer rate and thermal conductivity is represented by Bi, which is a dimensionless metric. The heat flux rises as Bi rises because more convection occurs as the Biot number rises, resulting in an increase in thermal boundary layer's thickness and temperature profile. Figure 12 indicates that the increment in Casson fluid parameter ($0.2 \le \beta \le 0.8$), temperature profile is increased. Physically this happened as the greater values of β designate stronger molecular motion and interactions that ultimately lead to an increase in the fluid temperature. In result, the thickness of thermal boundary layer is increased. The effect of the thermal relaxation parameter ($0 \le \Delta_T \le 0.3$) on temperature profile is shown in Figure 13. It is evident that increasing values of the thermal relaxation parameter, the fluid's temperature decreases (Rasool and Zhang [32]). The physical justification for this might be that by raising the thermal relaxation value, the material's particles need more time to transfer energy to its nearby neighbours. Therefore, a decrease in temperature profile is caused by rise in thermal relaxation parameter. Figure 14 depicts radiation parameter's ($0.1 \le R \le 1.5$) effect on thermal boundary layer. As radiation parameter R value rises, the radiative heat flow enhances, which increases thermal boundary layer's thickness and hence the temperature.

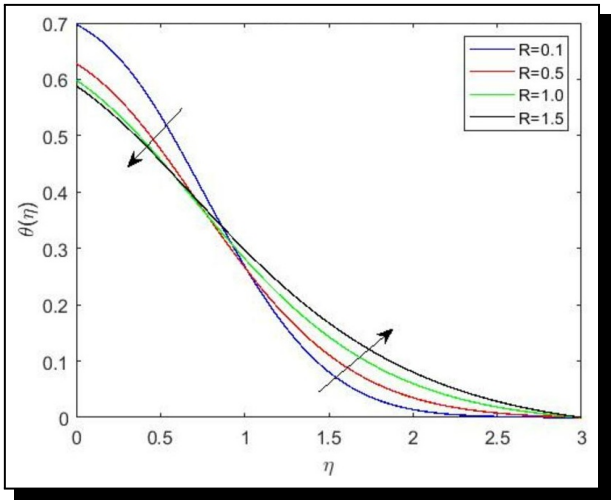

Figure 14. Variation in temperature for different R values

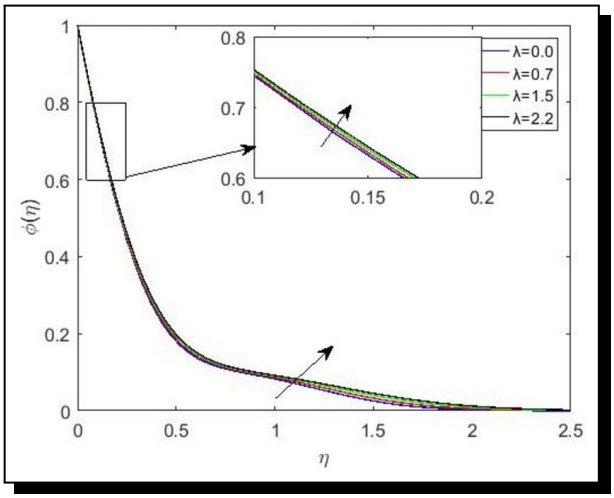

Figure 15. Variation in nanoparticle volume fraction for different λ values

The effects of different factors on volume fraction profile of nanoparticle are shown in Figures 15-21. In Figure 15, the concentration profile and concentration boundary layer's thickness both rise as the porosity parameter ($0 \le \lambda \le 2.2$) is increased. Because of the porosity parameter λ, mass diffusivity is larger, and $\phi(\eta)$ (Muhammad *et al*. [24]) rises. In Figure 16 the influence of parameter of Brownian motion ($0.3 \le Nb \le 1$) on the profile of concentration is shown. As the amount of Nb in the fluid grows, the thickness of boundary layer of concentration declines. Figure 17 shows the influence of thermophoresis parameter Nt between 0.1 and 0.7 on

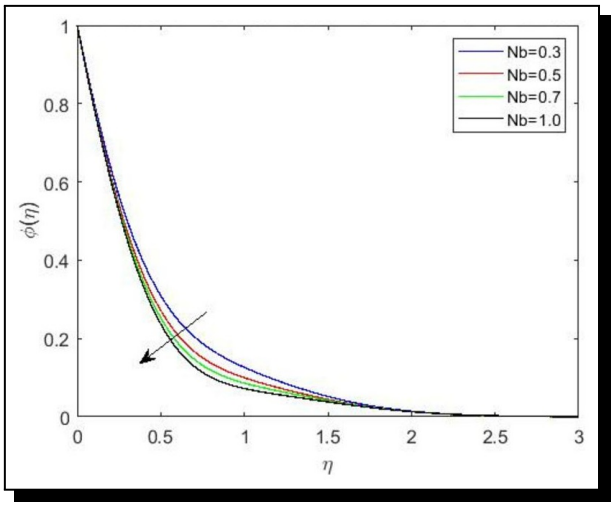

Figure 16. Variation in nanoparticle volume fraction for different Nb values

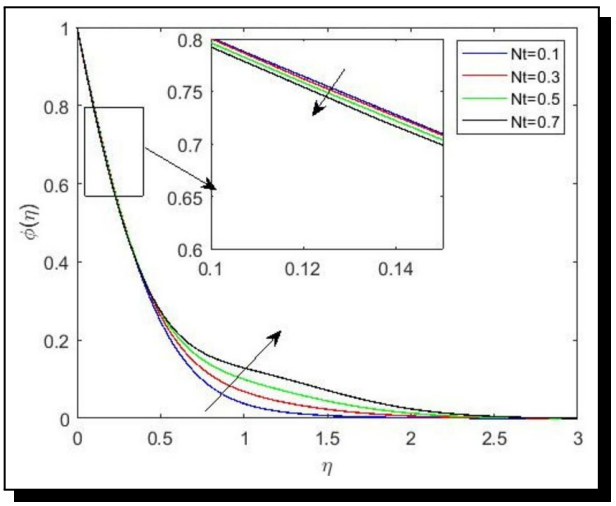

Figure 17. Variation in nanoparticle volume fraction for different Nt values

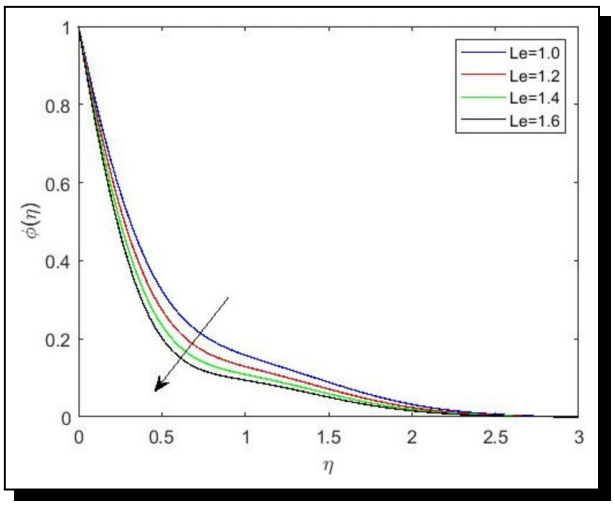

Figure 18. Variations in nanoparticle volume fraction for different Le values

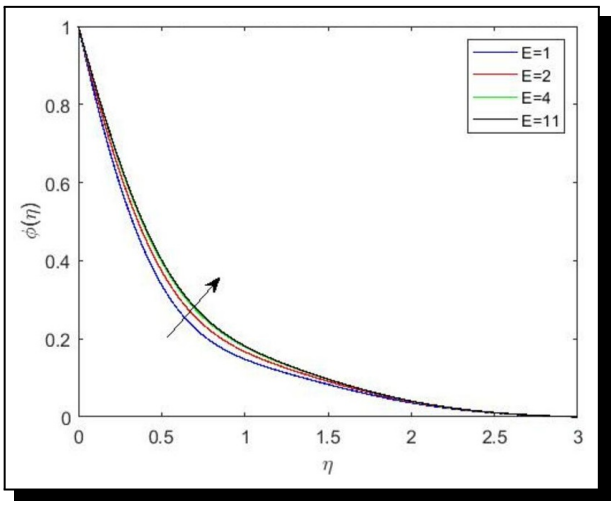

Figure 19. Variations in nanoparticle volume fraction for different E values

profile of nanoparticle volume fraction. The force of thermophoresis increases as Nt increases, transporting nanoparticles from hotter regions to colder ones, resulting in increase of thickness of concentration boundary layer. Figure 18 shows the effect of Lewis number ($1.0 \le Le \le 1.6$) on the profile of nanoparticle volume fraction. It shows that when Le grows, the mass diffusivity declines, and boundary layer thickness of concentration reduces. In Figure 19 we can see the effect of activation energy ($1 \le E \le 11$) on nanoparticle volume fraction profile. Growth in the thermophoresis parameter is related to the growth in temperature, which is linked to the growth in AE, resulting in a faster rate of chemical reaction and a higher concentration in boundary layer. As E increases, thickness of boundary layer of concentration rises. Figure 20 shows the influence of temperature difference ($0 \le \delta \le 7$) on profile of nanoparticle volume fraction. As the temperature difference increases, concentration boundary layer thickness decreases (Anuradha and Sashikala [2]). Enhancement of the chemical reaction parameter ($0 \le \sigma^* \le 1$) clearly result in a decrease in nanoparticle concentration [2]. An increase in values of σ^* causes the Arrhenius

expression to rise, which ultimately damages the chemical reaction.

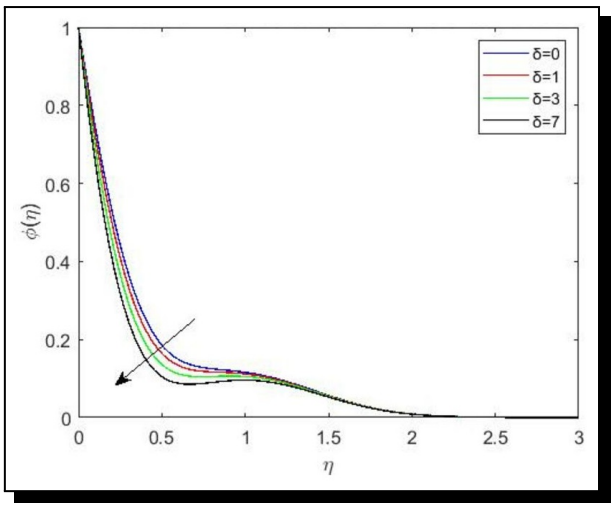

Figure 20. Variation in nanoparticle volume fraction for different δ values

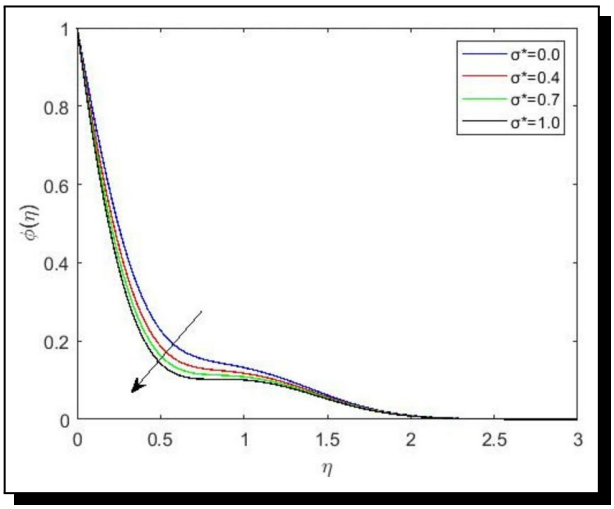

Figure 21. Variation in nanoparticle volume fraction for different σ^* values

The skin friction coefficient $[-(2Re_x)^{\frac{1}{2}}Cf_x]$ is matched to the previous results of Nadeem *et al*. [27], and Ullah *et al*. [40] in Table 1 for various Casson fluid parameter and Magnetic parameter values. The results got are seen in good accord with existing results. In Table 2, we matched the local Nusselt number $[-\theta'(0)]$ values for $Nt = 0.5$, $Sc = 20$, $Pr = 5$ with rest of the parameters as zero. The results achieved are found to be in good accord with existing results of Reddy and Naikoti [33].

Table 1. Comparing skin friction coefficient for various β and M values

M	β	Nadeem *et al*. [27]	Ullah *et al*. [40]	Present results
0	∞	1.0042	1	1
	5	1.0954	1.0955	1.0955
	1	1.4142	1.4144	1.4144
10	∞	3.3165	3.3166	3.3166
	5	3.6331	3.6332	3.6332
	1	4.6904	4.6904	4.6904
100	∞	10.049	10.0499	10.0499
	5	11.0091	11.0091	11.0091
	1	14.2127	14.2127	14.2127

Table 2. Comparing results for local Nusselt number $-\theta'(0)$

Nt	Sc	Pr	Reddy and Naikoti [33]	Present results
0.5	20	5	0. 09390887	0.09345

From Table 3 we can see that the Local skin friction coefficient inclines with β and declines with λ, M and Fr (Gangaiah *et al*. [15]). The skin friction coefficient is reduced as the porosity parameter is increased. Raising the porosity parameter reduces the fluid's drag and hence

increases flow retardation. From Table 4 we found that the value of local Nusselt number decline with enhancement in values of M, Nt, λ, Fr and β (Gangaiah *et al*. [15]) and opposite nature is observed with Pr and R. From Table 5 we found that local Sherwood number rises with growing Le, σ^*, Pr, Nt, δ_C (Rasool and Zhang [32]) and δ and declines with rising M, E, β, λ, and Fr.

Table 3. Skin Friction for different parameters

S. No.	M	β	Fr	λ	$(Re_x)^{\frac{1}{2}}Cf_x$
1	0	0.5			−2.212389
2		1			−1.766335
3		2			−1.515354
4	0.5	0.5			−2.504483
5		1			−2.017562
6		2			−1.738572
7	1	0.5			−2.773139
8		1			−2.245428
9		2			−1.939267
10			0	0	−1.881699
11				0.4	−2.095100
12				0.8	−2.292396
13			0.5	0	−2.062217
14				0.4	2.260961
15				0.8	−2.446296
16			1	0	−2.229849
17				0.4	−2.416468
18				0.8	−2.591705

Table 4. Nusselt Number for different parameters

S. No.	M	β	Fr	λ	Pr	Nt	R	$(Re_x)^{\frac{-1}{2}}Nu_x$
1	0.3							0.382025
2	0.6							0.325990
3	0.9							0.298917
4		0.5						0.387039
5		1						0.324195
6		2						0.293053
7			0					0.329257
8			0.3					0.327219
9			0.6					0.325273
10				0				0.383638
11				0.4				0.325990
12				0.8				0.275697
13					0.5			0.382084
14					1			0.401437
15					1.5			0.416115
16						0		0.327219
17						0.5		0.208522
18						1		0.062288
19							0.2	0.193608
20							0.4	0.241646
21							0.8	0.410148

4. Conclusions

The following are some of the work's concluding observations.

- The fluid velocity contour declines with an increment in the porosity parameter (Eswaramoorthi *et al.* [13], and Rasool and Zhang [32]), Forchheimer parameter, parameter of Casson fluid (Mukhopadhyay *et al.* [25]) and parameter of magnetic field (Waqas *et al.* [42]).
- Thickness of thermal boundary layer grows with rise in Biot number, porosity parameter, Forchheimer parameter, magnetic parameter, parameter of Brownian motion, Casson fluid parameter (Mukhopadhyay *et al.* [25]) and thermophoresis parameter (Hayat *et al.* [17]) and declines with thermal relaxation parameter.
- The nanoparticle volume fraction contour decrease with rising chemical reaction rate constant (Majeed *et al.* [22]), Lewis number Le, temperature difference, and enhances with the porosity parameter and AE [22].

Table 5. Sherwood Number for different parameters

S. No.	M	β	Fr	λ	Pr	Nt	σ^*	Le	E	δ	δ_C	$(Re_x)^{\frac{-1}{2}} Sh_x$
1	1											2.596630
2	2											2.453907
3	3											2.308125
4		2										2.526176
5		3										2.512501
6		4										2.335814
7			0									2.521422
8			0.5									2.508822
9			1									2.379233
10				0								2.408380
11				0.5								2.386260
12				1								2.366306
13					1.7							1.071372
14					5							2.068658
15					7							2.535372
16						0						2.286071
17						0.5						2.513726
18						1						2.679550
19							0.5	1				2.379192
20								1.2				2.513726
21								1.5				2.875223
22							1	1				2.688698
23								1.2				2.781524
24								1.5				3.185264
25							1.5	1				2.770795
26								1.2				3.007282
27								1.5				3.449902
28									0			2.856563
29									0.5			2.660234
20									1			2.513726
31									1.5			2.408619
32										0		2.450691
33										0.3		2.513726
34										0.6		2.572029
35											0	2.354890
36											0.05	2.374649
37											0.1	2.513726

- The coefficient of "skin friction" grew with the increment in Casson fluid parameter value (Mukhopadhyay *et al.* [25]) and decline with the rise in magnetic field parameter value (Shah *et al.* [38]), porosity parameter, and Forchheimer parameter.
- The local Nusselt number rises with the enhancement in the value of Prandtl number and radiation parameter (Sajid *et al.* [35]) whereas decreases with the increase in Casson fluid parameter value, Porosity parameter, Forchheimer parameter, and thermophoresis number.
- The local Sherwood number rises with the rise in Prandtl number, thermophoresis number, chemical reaction rate constant, Lewis number, Solute relaxation parameter (Rasool and Zhang [32]) and temperature difference whereas decreases with increment in magnetic field parameter, Forchheimer parameter, Casson fluid parameter, porosity parameter, and activation energy.

Competing Interests

The authors declare that they have no competing interests.

Authors' Contributions

All the authors contributed significantly in writing this article. The authors read and approved the final manuscript.

References

[1] W. Abbas and M. M. Magdy, Heat and mass transfer analysis of nanofluid flow based on Cu, Al_2O_3, and TiO_2 over a moving rotating plate and impact of various nanoparticle shapes, *Mathematical Problems in Engineering* 2020 (2020), Article ID 9606382, 12 pages, DOI: 10.1155/2020/9606382.

[2] S. Anuradha and K. Sashikala, MHD free convective flow of a nanofluid over a permeable shrinking sheet with binary chemical reaction and activation energy, *International Journal of Engineering Science Invention* **7**(1) (2018), 22 – 30, URL: http://www.ijesi.org/papers/Vol(7)i1/Version-1/D0701012230.pdf.

[3] E. M. Arthur, I. Y. Seini and L. B. Bortteir, Analysis of casson fluid flow over a vertical porous surface with chemical reaction in the presence of magnetic field, *Journal of Applied Mathematics and Physics* **3**(6) (2015), 713 – 723, DOI: 10.4236/jamp.2015.36085.

[4] S. M. Atif, S. Shah and A. Kamran, Effect of MHD on Casson fluid with Arrhenius activation energy and variable properties, *Scientia Iranica F* **29**(6) (2022), 3570 – 3581, DOI: 10.24200/SCI.2021.57873.5452.

[5] T. Aziz, F. M. Mahomed, A. Shahzad and R. Ali, Travelling wave solutions for the unsteady flow of a third grade fluid induced due to impulsive motion of flat porous plate embedded in a porous medium, *Journal of Mechanics* **30**(5) (2014), 527 – 535, DOI: 10.1017/jmech.2014.17.

[6] A. R. Bestman, Natural convection boundary layer with suction and mass transfer in a porous medium, *International Journal of Energy Research* **14**(4) (1990), 389 – 396, DOI: 10.1002/er.4440140403.

[7] M. Bilal, I. Khan, T. Gul, A. Tassaddiq, W. Alghamdi, S. Mukhtar and P. Kumam, Darcy-Forchheimer hybrid nano fluid flow with mixed convection past an inclined cylinder, *Computers, Materials & Continua* **66**(2) (2021), 2025 – 2039, DOI: 10.32604/cmc.2020.012677.

[8] N. Casson, A Flow equation for pigment-oil suspensions of the printing ink type, in: *Rheology of Disperse Systems*, C. C. Mill (editor), Pergamon Press, Oxford, pp. 84 – 104 (1959).

[9] S. Charm and G. Kurland, Viscometry of human blood for shear rates of 0-100,000 $\sec^{-1}$, *Nature* **206** (1965), 617 – 618, URL: https://www.nature.com/articles/206617a0.

[10] R. K. Dash, K. N. Mehta and G. Jayaraman, Casson fluid flow in a pipe filled with a homogeneous porous medium, *International Journal of Engineering Science* **34**(10) (1996), 1145 – 1156, DOI: 10.1016/0020-7225(96)00012-2.

[11] G. L. Devi, H. Niranjan and S. Sivasankaran, Effects of chemical reactions, radiation, and activation energy on MHD buoyancy induced nano fluidflow past a vertical surface, *Scientia Iranica B* **29**(1) (2022), 90 – 100, DOI: 10.24200/sci.2021.56835.4934.

[12] M. Dhlamini, P. K. Kameswaran, P. Sibanda, S. Motsa and H. Mondal, Activation energy and binary chemical reaction effects in mixed convective nanofluid flow with convective boundary conditions, *Journal of Computational Design and Engineering* **6**(2) (2019), 149 – 158, DOI: 10.1016/j.jcde.2018.07.002.

[13] S. Eswaramoorthi, N. Alessa, M. Sangeethavaanee, S. Kayikci and N. Namgyel, Mixed convection and thermally radiative flow of MHD Williamson nanofluid with Arrhenius activation energy and Cattaneo–Christov heat-mass flux, *Journal of Mathematics* **2021** (2021), Article ID 2490524, DOI: 10.1155/2021/2490524.

[14] N. V. Ganesh, A. K. A. Hakeem and B. Ganga, Darcy–Forchheimer flow of hydromagnetic nanofluid over a stretching/shrinking sheet in a thermally stratified porous medium with second order slip, viscous and Ohmic dissipations effects, *Ain Shams Engineering Journal* **9**(4) (2018), 939 – 951, DOI: 10.1016/j.asej.2016.04.019.

[15] T. Gangaiah, N. Saidulu and A. V. Lakshmi, The influence of thermal radiation on mixed convection MHD flow of a Casson nonfluid over an exponentially stretching sheet, *International Journal of Nanoscience and Nanotechnology* **15**(2) (2019), 83 – 98, URL: http://www.ijnnonline.net/article_35419.html.

[16] T. Hayat, F. Haider and A. Alsaedi, Darcy-Forchheimer flow with nonlinear mixed convection, *Applied Mathematics and Mechanics* **41** (2020), 1685 – 1696, DOI: 10.1007/s10483-020-2680-8.

[17] T. Hayat, F. Shah, Z. Hussain and A. Al-Saedi, Darcy-Forchheimer flow of Jeffrey nanofluid with heat generation/absorption and melting heat transfer, *Thermal Science* **23**(6) (Part B) (2019), 3833 – 3842, DOI: 10.2298/TSCI171222314H.

[18] C.-J. Huang, Arrhenius activation energy effect on free convection about a permeable horizontal cylinder in porous media, *Transport in Porous Media* **128** (2019), 723 – 740, DOI: 10.1007/s11242-019-01267-1.

[19] M. Ijaz, M. S. Alqarni, F. Salah and M. Y. Malik, Numerical simulation of Joule heating and Arrhenius activation energy for nonlinear radiative flow of Casson nanofluid with Cattaneo–Christov heat flux model, *Physica Scripta* **95**(2) (2020), 025401, DOI: 10.1088/1402-4896/ab41ac.

[20] S. Jabeen, T. Hayat, S. Qayyum and A. Alsaedi, Significance of activation energy in stratified flow of tangent hyperbolic fluid, *International Journal of Numerical Methods for Heat & Fluid Flow* **29**(8) (2019), 2932 – 2947, DOI: 10.1108/HFF-12-2018-0795.

[21] M. Jawad, A. Saeed, T. Gul and A. Bariq, MHD Darcy-Forchheimer flow of Casson nanofluid due to a rotating disk with thermal radiation and Arrhenius activation energy, *Journal of Physics Communications* **5**(2) (2021), 025008, DOI: 10.1088/2399-6528/abe4e0.

[22] A. Majeed, F. M. Noori, A. Zeeshan, T. Mahmood, S. U. Rehman and I. Khan, Analysis of activation energy in magnetohydrodynamic flow with chemical reaction and second order momentum slip model, *Case Studies in Thermal Engineering* **12** (2018), 765 – 773, DOI: 10.1016/j.csite.2018.10.007.

[23] K. A. Maleque, Effects of binary chemical reaction and activation energy on MHD boundary layer heat and mass transfer flow with viscous dissipation and heat generation/absorption, *International Scholarly Research Notices* **2013** (2013), Article ID 284637, 9 pages, DOI: 10.1155/2013/284637.

[24] T. Muhammad, A. Alsaedi, S. A. Shehzad and T. Hayat, A revised model for Darcy-Forchheimer flow of Maxwell nanofluid subject to convective boundary condition, *Chinese Journal of Physics* **55**(3) (2017), 963 – 976, DOI: 10.1016/j.cjph.2017.03.006.

[25] S. Mukhopadhyay, K. Vajravelu and R. A. V. Gorder, Casson fluid flow and heat transfer at an exponentially stretching permeable surface, *Journal of Applied Mechanics* **80**(5) (2013), 054502, DOI: 10.1115/1.4023618.

[26] M. Mustafa, J. A. Khan, T. Hayat and A. Alsaedi, Buoyancy effects on the MHD nanofluid flow past a vertical surface with chemical reaction and activation energy, *International Journal of Heat and Mass Transfer* **108**(Part B) (2017), 1340 – 1346, DOI: 10.1016/j.ijheatmasstransfer.2017.01.029.

[27] S. Nadeem, R. U. Haq and N. S. Akbar, MHD three-dimensional boundary layer flow of Casson nanofluid past a linearly stretching sheet with convective boundary condition, *IEEE Transactions on Nanotechnology* **13**(1) (2014), 109 – 115, DOI: 10.1109/TNANO.2013.2293735.

[28] K. V. Prasad, H. Vaidya, K. Vajravelu and V. Ramanjini, Analytical study of Cattaneo-Christov heat flux model for Williamson-Nanofluid flow over a slender elastic sheet with variable thickness, *Journal of Nanofluids* **7**(3) (2018), 583 – 594, DOI: 10.1166/jon.2018.1475.

[29] K. Rafique, M. I. Anwar, M. Misiran, I. Khan, S. O. Alharbi, P. Thounthong and K. S. Nisar, Numerical solution of Casson nanofluid flow over a non-linear inclined surface with Soret and Dufour effects by Keller-Box method, *Frontiers in Physics* **7** (2019), Article 139, DOI: 10.3389/fphy.2019.00139.

[30] K. V. Ramana, K. Gangadhar, T. Kannan and A. J. Chamkha, Cattaneo–Christov heat flux theory on transverse MHD Oldroyd-B liquid over nonlinear stretched flow, *Journal of Thermal Analysis and Calorimetry* **147** (2022), 2749 – 2759, DOI: 10.1007/s10973-021-10568-x.

[31] G. K. Ramesh, Darcy-Forchheimer flow of Casson nanofluid with heat source/sink: A three-dimensional study, in: *Heat and Mass Transfer – Advances in Modelling and Experimental Study for Industrial Applications*, Y. Ren (editor), *IntechOpen*, London, 158 pages (2018), DOI: 10.5772/intechopen.74170.

[32] G. Rasool and T. Zhang, Darcy-Forchheimer nanofluidic flow manifested with Cattaneo-Christov theory of heat and mass flux over non-linearly stretching surface, *PLoS ONE* **14**(8) (2019), e022130, DOI: 10.1371/journal.pone.0221302.

[33] C. S. Reddy and K. Naikoti, MHD boundary layer flow of Casson nanofluid over a non linear stretching sheet with viscous dissipation and convective condition, *Journal of Nanofluids* **5**(6) (2016), 870 – 879, DOI: 10.1166/jon.2016.1271.

[34] S. R. R. Reddy, P. B. A. Reddy and A. M. Rashad, Effectiveness of binary chemical reaction on magneto-fluid flow with Cattaneo–Christov heat flux model, *Proceedings of the Institution of Mechanical Engineers, Part C: Journal of Mechanical Engineering Science* **235**(12) (2021), 2192 – 2200, DOI: 10.1177/0954406220950347.

[35] T. Sajid, M. Sagheer, S. Hussain and M. Bilal, Darcy-Forchheimer flow of Maxwell nanofluid flow with nonlinear thermal radiation and activation energy, *AIP Advances* **8** (2018), 035102, DOI: 10.1063/1.5019218.

[36] D. Sarve, P. K. Gaur and V. K. Sharma, Numerical simulation for activation energy impact on Darcy-Forchheimer flow of casson fluid suspended with nano particles over a stretching cylinder, *Science & Technology Asia* **26**(4) (2021), 106 – 114, URL: https://ph02.tci-thaijo.org/index.php/SciTechAsia/article/view/245885.

[37] D. U. Sarwe, B. Shanker, R. Mishra, R. S. Varun Kumar and M. N. R. Shekar, Simultaneous impact of magnetic and Arrhenius activation energy on the flow of Casson hybrid nanofluid over a vertically moving plate, *International Journal of Thermofluid Science and Technology* **8**(2) (2020), paper number 080202, DOI: 10.36963/IJTST.2021080202.

[38] Z. Shah, P. Kumam and W. Deebani, Radiative MHD Casson nanofluid flow with Activation energy and chemical reaction over past nonlinearly stretching surface through Entropy generation, *Scientific Reports* **10** (2020), Article number: 4402, DOI: 10.1038/s41598-020-61125-9.

[39] N. Thamaraikannan, S. Karthikeyan, D. K. Chaudhary and S. Kayikci, Analytical investigation of magnetohydrodynamic non-newtonian type casson nanofluid flow past a porous channel with periodic body acceleration, *Complexity* **2021** (2021), Article ID 7792422, 17 pages, DOI: 10.1155/2021/7792422.

[40] I. Ullah, I. Khan and S. Shafie, MHD natural convection flow of casson nanofluid over nonlinearly stretching sheet through porous medium with chemical reaction and thermal radiation, *Nanoscale Research Letters* **11** (2016), Article number: 527, DOI: 10.1186/s11671-016-1745-6.

[41] W. P. Walwander T. Y. Chen and D. F. Cala, An approximate Casson fluid model for tube flow of blood, *Biorheology* **12**(2) (1975), 111 – 119, DOI: 10.3233/BIR-1975-12202.

[42] M. Waqas, S. Naz, T. Hayat and A. Alsaedi, Numerical simulation for activation energy impact in Darcy–Forchheimer nanofluid flow by impermeable cylinder with thermal radiation, *Applied Nanoscience* **9**(5) (2019), 1173 – 1182, DOI: 10.1007/s13204-018-00940-z.

[43] M. Younus and A. V. Lakshmi, Numerical investigation of activation energy of radiative magnetohydrodynamic Williamson nanofluid flow, *Heat Transfer* **51**(7) (2022), 6197 – 6222, DOI: 10.1002/htj.22588.